Mechanics of Materials 190 (2024) 104912

Contents lists available at ScienceDirect

Mechanics of Materials

journal homepage: www.elsevier.com/locate/mecmat

Research paper

Constitutive models for confined elastomeric layers: Effects of nonlinearity and compressibility

Sida Hao [a], Rui Huang [a,*], Gregory J. Rodin [a,b]

[a] Department of Aerospace Engineering and Engineering Mechanics, University of Texas, Austin, TX, 78712, USA
[b] Oden Institute, University of Texas, Austin, TX, 78712, USA

ARTICLE INFO

Keywords:
Elastomer
Thin layer
Modeling error
Compressibility
Nonlinearity

ABSTRACT

Elastomers tend to undergo large deformations accompanied by small volumetric changes. For elastomeric layers sandwiched between rigid plates, large deformations can be significantly limited by the constraints imposed by the plates. Further, those constraints can be enhanced by material's inability to undergo large volumetric changes. From this perspective, it is appropriate to examine the validity of constitutive models, in which an elastomer is treated as incompressible, for analysis of the confined layers. Here, this issue is addressed by considering the mechanical response of sandwiched elastomeric layers using three constitutive models. The first one, referred to as compressible neo-Hookean, is regarded as exact. The other two models are regarded as approximations. Of those two, the first one neglects nonlinearity and the second one neglects compressibility. Accordingly, the modeling errors associated with the former are treated as measures of importance of nonlinearity, and the modeling errors associated with the latter are treated as measures of importance of compressibility. The modeling errors are evaluated using the force–displacement curve and the mean stress at the layer center as the quantities of interest. Numerical results are presented for rubber and polydimethylsiloxane (PDMS), characterized by Poisson's ratios $\nu = 0.4999$ and $\nu = 0.49$, respectively. It is shown that, even when the forces applied to the plates are large, considering nonlinearity is important for thick but not for thin layers. In contrast, considering compressibility is important for thin layers. The need for considering compressibility is further assessed by introducing a competition parameter, which reinforces the notion that compressibility is important for modeling PDMS layers and thin rubber layers.

1. Introduction

This paper is concerned with thin elastomeric layers sandwiched between stiff plates (Fig. 1). Such arrangements are used in numerous devices and structures for vibration isolation and shock absorption (Kelly and Konstantinidis, 2011; Warn and Ryan, 2012). In a laboratory setting, the arrangement is commonly referred to as the poker-chip specimen. Its use was pioneered by Gent and Lindley (1957, 1959), who recognized that poker-chip specimens are well suited for inducing large tensile stresses in thin rubber layers. As a result, poker-chip and closely-related specimens have been widely used for studying nucleation and growth of cavities and cracks in elastomers (Lindsey, 1967; Stringfellow and Abeyaratne, 1989; Gent, 1990; Fond, 2001; Bayraktar et al., 2008; Lefèvre et al., 2015; Kumar and Lopez-Pamies, 2021; Hao et al., 2023; Guo and Ravi-Chandar, 2023), and for studying adhesive bonding/debonding of soft elastic thin layers (Lin et al., 2000; Webber et al., 2003; Minsky and Turner, 2015; Fischer et al., 2017; Hensel et al., 2019; Benvidi and Bacca, 2021).

In this paper, we consider poker-chip specimens subjected to tension, focusing on the interplay between the layer thinness and the material compressibility. The former is defined as

$$\xi := \frac{h}{a}, \tag{1}$$

where h is the half thickness and a is the radius of the layer (Fig. 1). It is clear that the constraints imposed on the layer by the plates are particularly strong when $\xi \ll 1$. The effects of the constraints are dramatically amplified if the material is treated as incompressible, as it is done for fluid thin layers (Stefan, 1874; Reynolds, 1886). While this assumption is regarded as excessively restrictive in linear elastic analyses of poker-chip specimens (Lindsey et al., 1963; Lindley, 1979; Chalhoub and Kelly, 1990; Gent, 1994; Auslender et al., 1999; Lin et al., 2000; Qiao and Lu, 2015; Schapery, 2018a,b; Hensel et al., 2019; Benvidi and Bacca, 2021; Movchan et al., 2021, 2023), it is well established that many elastomers are nearly incompressible. For example, for variants of polydimethylsiloxane (PDMS), Poisson's ratio

* Corresponding author.
E-mail address: ruihuang@mail.utexas.edu (R. Huang).

https://doi.org/10.1016/j.mechmat.2024.104912
Received 12 September 2023; Received in revised form 7 January 2024; Accepted 8 January 2024
Available online 9 January 2024

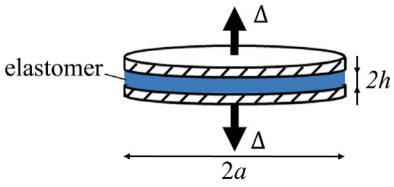

Fig. 1. A schematic of a poker-chip specimen.

ν varies between 0.45 and 0.5 (Müller et al., 2019), and for a typical rubber $\nu = 0.4999$ (Anderson et al., 2004). Since $\nu = 0.5$ implies incompressibility, the range between 0.45 and 0.5 can be regarded as representative values of Poisson's ratio for nearly incompressible materials. Ironically, in nonlinear elastic analyses of poker-chip specimens, it is common to treat the material as incompressible (Klingbeil and Shield, 1966; Lefèvre et al., 2015; Guo and Ravi-Chandar, 2023; Hao et al., 2023). Thus, among existing models, one class neglects material nonlinearity, whereas the other class neglects material compressibility. Addressing this chasm constitutes the goal of this work.

To assess the role of nonlinearity and compressibility of the constitutive model in analyses of poker-chip specimens, we consider three models. The first model accounts for both nonlinearity and compressibility, and it is regarded as exact. The other two models are regarded as approximate, as one neglects nonlinearity and the other neglects compressibility. Then, the differences in predictions based on the exact versus approximate models are adopted for quantifying modeling errors associated with the approximations that neglect nonlinearity or compressibility. For the first approximate model the choice is obvious — classical linear elasticity. In contrast, there is no obvious choice for the second approximate model, as the catalog of nonlinear elastic constitutive equations is quite substantial (Ogden, 1997). Nevertheless, for demonstration purposes, a natural choice is the incompressible neo-Hookean model. The advantage of this, frequently used and most frequently criticized, model is its simplicity, as it contains only one material parameter, the shear modulus μ. This simplicity is critically important for parametric studies. The incompressible neo-Hookean model is straightforward to generalize to the compressible one (Anand and Govindjee, 2020), which we adopt as the exact model. This model contains one more parameter, the bulk modulus κ. Of course, for infinitesimal deformations, the compressible neo-Hookean model reduces to linear elasticity, with two elastic constants, μ and κ. In what follows, we do not necessarily advocate for the compressible neo-Hookean model for any specific materials. Rather, our focus is to demonstrate that one needs to exercise caution in adopting the assumptions of either linearity or incompressibility in the analysis of elastomeric thin layers.

Our approach is based on finite element analysis. This allows us to control numerical errors and focus on modeling errors. Further, in contrast to approximate closed-form solutions, our approach is robust as it allows us to analyze both thin and moderately thick layers ($\xi \leq 0.5$), as commonly used in experiments (Gent and Lindley, 1959; Bayraktar et al., 2008; Guo and Ravi-Chandar, 2023).

The remainder of this paper is structured as follows. In Section 2, we formulate the boundary value problem for a poker-chip specimen. In Section 3, we present results for the case of rubber layers using the three aforementioned constitutive models. In Section 4, we present results for PDMS layers. In Section 5, we examine local stress states pertinent to the onset of cavitation or fracture in experiments. In Section 6, we discuss a competition between the layer thinness and material compressibility. We close the paper by recapturing key results in Section 7.

2. Problem statement

Consider a circular cylindrical layer sandwiched between two rigid plates. The layer is bonded to the plates and stretched by pulling the plates apart along the cylindrical axis, so that the upper plate is displaced by Δ and the lower plate by $-\Delta$ (Fig. 1).

We consider layers characterized by three well-established elastic constitutive models. The most general model considered in this work is compressible neo-Hookean (Ogden, 1997; Basar and Weichert, 2000; Pence and Gou, 2015; Anand and Govindjee, 2020). This model is based on the strain energy density function

$$W = \frac{1}{2}\mu\left(\bar{I}_1 - 3\right) + \frac{1}{2}\kappa(J-1)^2 . \tag{2}$$

Here the scalars J and $\bar{I}_1$ are defined via the deformation gradient $\mathbf{F}$ as

$$J := \det \mathbf{F} \tag{3}$$

and

$$\bar{I}_1 := J^{-\frac{2}{3}} F_{ij} F_{ij} . \tag{4}$$

On the right-hand side of (2), the first term represents the deviatoric (or isochoric) response, and the second term represents the isotropic (or dilatational) response. Accordingly, it is expedient to split the true stress tensor corresponding to (2) into the deviatoric and isotropic components:

$$\sigma_{ij} = s_{ij} - p\delta_{ij} , \tag{5}$$

where s_{ij} is the deviatoric stress and p is the pressure. Then, the strain energy density function (2) leads to the constitutive equations

$$s_{ij} = \mu J^{-\frac{5}{3}}\left(F_{ik}F_{jk} - \frac{1}{3}F_{lk}F_{lk}\delta_{ij}\right) \tag{6}$$

and

$$p = -\kappa\,(J-1) . \tag{7}$$

Here, the pressure is taken to be linearly proportional to the volumetric strain $J-1$. This is justified by the fact that the volumetric strain is typically small (but not zero) in the confined elastomeric layers.

The other two models are particular cases of the compressible neo-Hookean model. Of those two, the first one is obtained by assuming that the deformation is small so that the displacement gradient $|\nabla \mathbf{u}| \ll 1$. With this assumption, (6) and (7) are reduced to the constitutive equations of linear elasticity:

$$s_{ij} = \mu\left(u_{i,j} + u_{j,i} - \frac{2}{3}\delta_{ij}u_{k,k}\right) \tag{8}$$

and

$$p = -\kappa u_{k,k} . \tag{9}$$

Thus, μ and κ are the standard material constants of linear elasticity. To this end, we recall the identity,

$$\frac{\kappa}{\mu} = \frac{2(1+\nu)}{3(1-2\nu)} ,$$

which characterizes the material compressibility. A nearly incompressible material can be associated with either $\nu \approx 0.5$ or $\kappa/\mu \gg 1$.

The third model is obtained by assuming that the material is incompressible, so that $\kappa/\mu \to \infty$ and $J = 1$. As a result, (6) is reduced to

$$s_{ij} = \mu\left(F_{ik}F_{jk} - \frac{1}{3}F_{lk}F_{lk}\delta_{ij}\right) . \tag{10}$$

The pressure p, however, cannot be determined from (7). Rather, it is determined from equilibrium conditions.

Since the plates are considered rigid and perfectly bonded to the layer, the boundary conditions on the flat surfaces of the layer are specified as

$$u_i\left[x_1, x_2, \pm(h+\Delta)\right] = \pm\delta_{i3}\Delta . \tag{11}$$

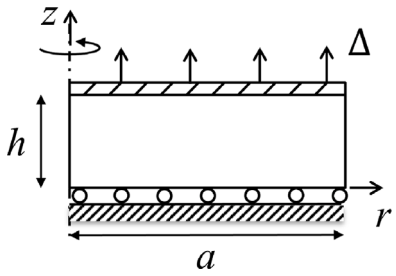

Fig. 2. An axisymmetric model for the upper half of the layer.

These boundary conditions are prescribed in the deformed configuration. On the cylindrical surface, the traction-free boundary condition implies that

$$\sigma_{ij} n_j = 0\,. \tag{12}$$

In this work, we identify the force F, required to produce the displacement Δ, as a quantity of interest. The relationship between F and Δ describes the overall response of the constrained layer and the apparent stiffness of the material.

Numerical results are obtained by finite element analysis using ABAQUS. A typical analysis involves an axisymmetric boundary-value problem (Fig. 2). Such problems do not pose significant challenges and can be accurately solved using standard ABAQUS options. In particular, we discretized the upper half of the layer using meshes comprised of eight-node hybrid (CAX8H) elements for handling the incompressible and nearly incompressible constitutive models, so that finite element discretization errors were estimated to be less than 10^{-3}. Due to symmetry, only the upper half of the layer was modeled. Accordingly, the boundary conditions on the lower surface were replaced by the symmetry conditions on the mid-plane of the layer at $z = 0$:

$$\sigma_{rz} = 0 \quad \text{and} \quad u_z = 0\,. \tag{13}$$

Here we use cylindrical rather than Cartesian components, which are more natural for axisymmetric problems (Fig. 2).

3. Analysis of rubber layers

In this section, we focus on analyzing rubber layers. Following Anderson et al. (2004), a typical rubber is characterized by $\nu = 0.4999$, which implies the ratio

$$\frac{\kappa}{\mu} = 5000. \tag{14}$$

Let us introduce the following dimensionless quantities

$$\hat{\Delta} := \frac{\Delta}{h} \tag{15}$$

and

$$\hat{F} := \frac{F}{\pi a^2 \mu}\,. \tag{16}$$

Note that $\hat{\Delta}$ is the average axial strain, and $\hat{F}$ is the average axial stress normalized by the shear modulus.

Since κ/μ has been fixed for the rubber layers, $\hat{F}$ can be described by a dimensionless function of ξ and $\hat{\Delta}$:

$$\hat{F} = f\left(\xi, \hat{\Delta}\right)\,. \tag{17}$$

Because we consider three constitutive models, there are three versions of the function $f\left(\xi, \hat{\Delta}\right)$. The function f obtained using the compressible neo-Hookean model is denoted by $f^{(0)}$, and it is treated as the benchmark. The functions f corresponding to the linear and incompressible neo-Hookean models are denoted by $f^{(1)}$ and $f^{(2)}$, respectively. These

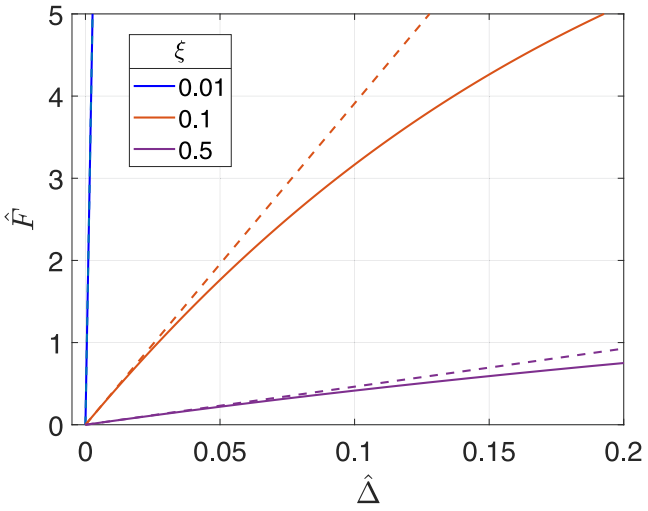

Fig. 3. Normalized force–displacement curves corresponding to the linear (dashed lines) and nonlinear, compressible neo-Hookean (solid lines) models for $\xi = 0.01$ (blue), 0.1 (red), and 0.5 (purple). (For interpretation of the references to color in this figure legend, the reader is referred to the web version of this article.)

two functions are treated as approximations, and therefore we define two modeling errors:

$$e^{(1)}\left(\xi, \hat{\Delta}\right) := \left| \frac{f^{(1)}\left(\xi, \hat{\Delta}\right) - f^{(0)}\left(\xi, \hat{\Delta}\right)}{f^{(0)}\left(\xi, \hat{\Delta}\right)} \right| \tag{18}$$

and

$$e^{(2)}\left(\xi, \hat{\Delta}\right) := \left| \frac{f^{(2)}\left(\xi, \hat{\Delta}\right) - f^{(0)}\left(\xi, \hat{\Delta}\right)}{f^{(0)}\left(\xi, \hat{\Delta}\right)} \right|\,. \tag{19}$$

Thus, $e^{(1)}$ is a measure of the importance of nonlinearity, and $e^{(2)}$ is a measure of the importance of compressibility.

3.1. Nonlinearity

In this subsection, we focus on the importance of nonlinearity, by comparing the numerical results obtained from the compressible neo-Hookean model to those from the linear elastic model. Let us begin with the results presented in Fig. 3, where normalized force–displacement curves predicted by the two models are plotted for $\xi = 0.01, 0.1, 0.5$. The predictions of the linear model are shown as dashed lines, and those of the nonlinear model by solid lines. Note that, for the thinnest layer ($\xi = 0.01$), the two curves are nearly identical for $\hat{F}$ up to five, which corresponds to a very large average axial stress equal to 5 μ. The proximity of the two curves can be explained, once we observe that the average axial strain $\hat{\Delta}$ corresponding to this stress level is less than 0.3%. In contrast, the two curves are significantly different for the thicker layers ($\xi = 0.1, 0.5$), which are much more compliant than the thinnest layer, and therefore undergo larger deformations. Thus, the comparisons in Fig. 3 suggest that the importance of nonlinearity increases as ξ increases.

Next, we evaluate the modeling error $e^{(1)}$ in the parametric hyperplane spanned by ξ and $\hat{\Delta}$. To this end, we plot contours of constant $e^{(1)}$ values for $e^{(1)} = 0.01, 0.05, 0.10$ (Fig. 4(a)). In this figure, the region below the contour $e^{(1)} = 0.01$ is characterized by $e^{(1)} < 0.01$. Therefore, for all points in this region, one can predict the function $f\left(\xi, \hat{\Delta}\right)$ with less than one percent error using the linear elastic model. The same logic applies to the contours $e^{(1)} = 0.05, 0.10$. Evidently, the importance of nonlinearity increases as the average axial strain $\hat{\Delta}$ increases.

It is instructive to plot contours of constant $e^{(1)}$ in the parametric hyperplane spanned by ξ and $\hat{F}$. To this end, we transform the ordinate axis in Fig. 4(a) using the force–displacement relation (17). The

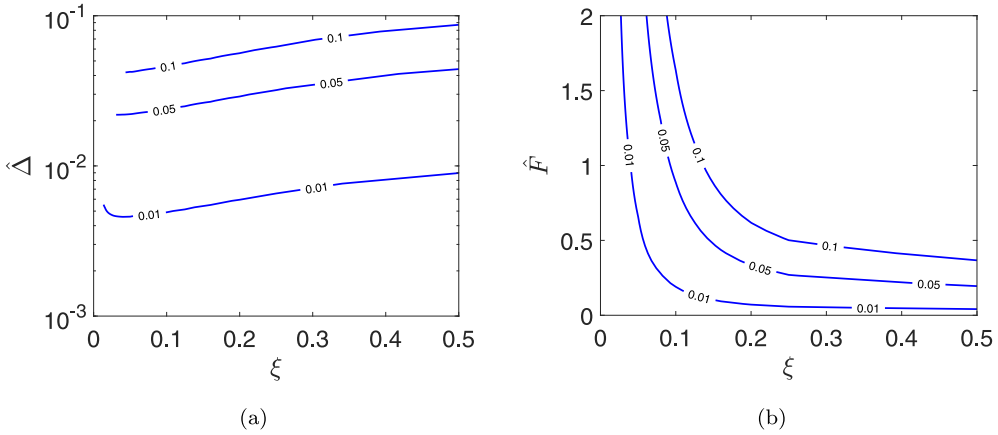

Fig. 4. Contours of the modeling error $e^{(1)}$ in two hyperplanes: (a) $\xi - \hat{\Delta}$ and (b) $\xi - \hat{F}$.

transformed contours are shown in Fig. 4(b). The seemingly qualitative difference between the contours in Fig. 4(b) versus those in Fig. 4(a) is due to the rapid increase in the apparent stiffness of the specimen as ξ decreases. As a result, the modeling error $e^{(1)}$ remains low for thin layers even when the average axial stress $\hat{F}$ is large. At a constant $\hat{F}$, the importance of nonlinearity increases with ξ.

3.2. Compressibility

In this subsection, we focus on the importance of compressibility, and therefore compare predictions based on the compressible neo-Hookean model versus incompressible neo-Hookean model. We begin with Fig. 5 which shows the normalized force–displacement curves for $\xi = 0.01, 0.1$, and 0.5. The predictions corresponding to the incompressible neo-Hookean model are shown in dashed lines, and those corresponding to the compressible neo-Hookean model are shown in solid lines. Contrary to the linear model, the incompressible neo-Hookean model shows better agreement with the compressible neo-Hookean model for the thick layer ($\xi = 0.5$) than the thin layer ($\xi = 0.01$). Thus, the importance of compressibility diminishes as ξ increases. Note that, for the thinnest layer ($\xi = 0.01$), the normalized force–displacement curves are nearly linear up to $\hat{F} = 5$ by both the compressible and incompressible models, but the slopes are different (approximately by a factor of 2).

Next, we evaluate the modeling error $e^{(2)}$ in the parametric hyperplane spanned by ξ and $\hat{\Delta}$. The contours of constant $e^{(2)}$ are plotted in Fig. 6 for $e^{(2)} = 0.01, 0.05, 0.10$. In this figure, all points located in the region to the right of the contour $e^{(2)} = 0.01$ are characterized by $e^{(2)} < 0.01$. Therefore, for those points, one can predict $f\left(\xi, \hat{\Delta}\right)$ with less than one percent error using the incompressible neo-Hookean model. The same logic applies to the contours $e^{(2)} = 0.05, 0.10$. It is clear that the contours are almost independent of $\hat{\Delta}$, and $e^{(2)}$ increases as ξ decreases. Therefore, the importance of compressibility increases as ξ decreases for thin layers. For moderately thick rubber layers with $\xi > 0.1$, the role of compressibility diminishes.

3.3. Maps

In this subsection, we combine results presented in the two previous subsections to construct maps of validity for the two approximate models. To this end, we set the error tolerances $e^{(1)} = 0.01$ and $e^{(2)} = 0.01$. The map plotted in the hyperplane spanned by ξ and $\hat{\Delta}$ is shown in Fig. 7(a). There one can identify four regions. In Region I (red), $e^{(1)} > 0.01$ and $e^{(2)} > 0.01$, and therefore neither linear nor incompressible neo-Hookean models are acceptable. In Region II (yellow), $e^{(1)} < 0.01$ but $e^{(2)} > 0.01$, and therefore the linear model is acceptable but the incompressible neo-Hookean model is not. In Region III (orange), $e^{(2)} <$

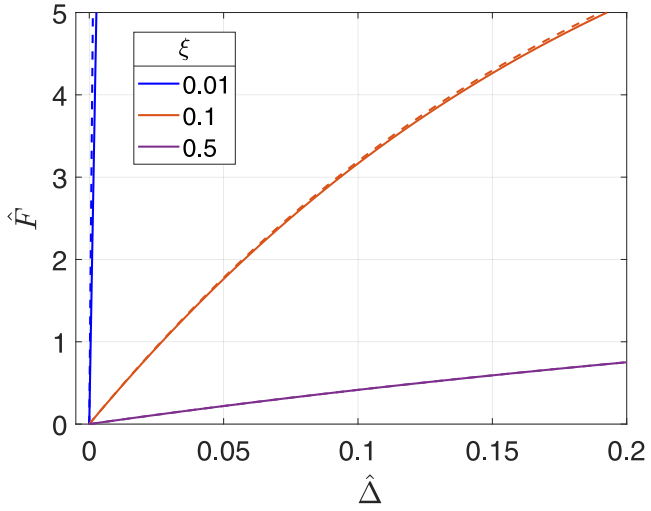

Fig. 5. Normalized force–displacement curves corresponding to the incompressible (dashed lines) and compressible (solid lines) neo-Hookean models for $\xi = 0.01$ (blue), $\xi = 0.1$ (red), and $\xi = 0.5$ (purple). (For interpretation of the references to color in this figure legend, the reader is referred to the web version of this article.)

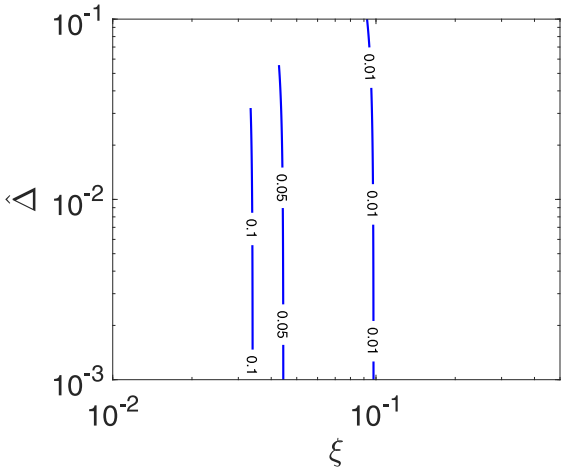

Fig. 6. Contours of the modeling error $e^{(2)}$ in the hyperplane $\xi - \hat{\Delta}$.

0.01 but $e^{(1)} > 0.01$, and therefore the incompressible neo-Hookean model is acceptable but the linear model is not. Finally, in Region IV (green), $e^{(1)} < 0.01$ and $e^{(2)} < 0.01$, and therefore both linear and

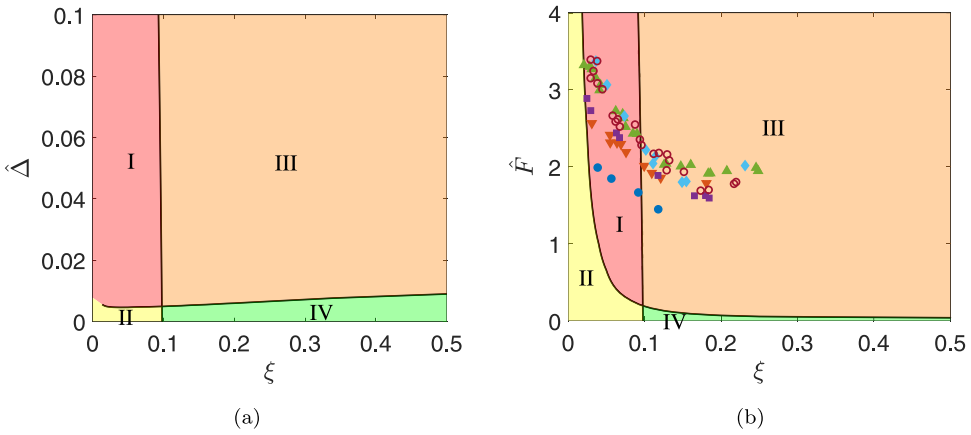

Fig. 7. Model validity maps for rubber layers in two hyperplanes: (a) $\xi - \hat{\Delta}$ and (b) $\xi - \hat{F}$. Error tolerances for both $e^{(1)}$ and $e^{(2)}$ are set at 1%. In Region I (red), neither the linear nor the incompressible neo-Hookean model is acceptable. In Region II (yellow), the linear model is acceptable but the incompressible model is not. In Region III (orange), the incompressible neo-Hookean model is acceptable but the linear model is not. In Region IV (green), both the linear and incompressible models are acceptable. Discrete symbols in (b) represent experimental data of critical forces for cavitation in rubber layers from Gent and Lindley (1959). (For interpretation of the references to color in this figure legend, the reader is referred to the web version of this article.)

incompressible neo-Hookean models are acceptable. The map confirms that compressibility is important only for thin rubber layers ($\xi < 0.1$), whereas, for all layers, nonlinearity is important when the average axial strain is large (roughly, $\hat{\Delta} > 0.01$).

One can also interpret the map by recognizing that the union of Regions I and III is separated from the union of Regions II and IV by the contour $e^{(1)} = 0.01$. Similarly, the union of Regions I and II is separated from the union of Regions III and IV by the contour $e^{(2)} = 0.01$. In the map, these two curves have only one intersection, and therefore there are four regions.

The map in Fig. 7(a) can be transformed into the map plotted in the hyperplane spanned by ξ and $\hat{F}$ (Fig. 7(b)), using the force–displacement relation (17). The advantage of the new map is that it allows us to establish a link with the experimental data compiled by Gent and Lindley (1959). Those data are shown as discrete symbols, and each point represents a critical force associated with the onset of cavitation in a rubber layer. We use six types of symbols to emphasize that the data were collected for six distinctly different rubbers. It is remarkable that the data are confined to a relatively narrow region of the $\xi - \hat{F}$ hyperplane. Fig. 7(b) clearly demonstrates that (i) for all the data, nonlinearity should be taken into account before the onset of cavitation, and (ii) for a large portion of the data, compressibility should be taken into account, due to the thinness of the rubber layers ($\xi < 0.1$).

It is instructive to construct a map in the $\xi - \hat{F}$ hyperplane, using the error tolerance 10% rather than 1% (Fig. 8). This map is qualitatively different from that shown in Fig. 7(b). In particular, the new map does not include Region I, where both approximate models are unacceptable. Region IV, where both the linear model and incompressible neo-Hookean model are acceptable, has been expanded significantly in comparison to its counterpart in Fig. 7(b), because of the larger error tolerance for both $e^{(1)}$ and $e^{(2)}$. This can be understood by observing that the contour $e^{(1)} = 0.1$ is above and to the right of the contour $e^{(1)} = 0.01$ in Fig. 4(b). Also, the contour $e^{(2)} = 0.1$ is to the left of the contour $e^{(2)} = 0.01$ in Fig. 6. As a result, the two curves for $e^{(1)} = 0.1$ and $e^{(2)} = 0.1$ do not intersect on the map shown in Fig. 8 (although they would intersect at a much higher force level not displayed here), and thus Region I disappears. The same symbols for the experimental data shown in Fig. 7(b) are shown in Fig. 8. Now, with the error tolerance $e^{(2)} = 0.1$, the incompressible neo-Hookean model is acceptable for most of the data, except for a small number of cases involving very thin layers ($\xi < 0.03$). Similarly, with the error tolerance $e^{(1)} = 0.1$, the linear model is acceptable for most of the thin layers with $\xi < 0.1$, even though the normalized forces are fairly high. Therefore, the validity of the approximate models depends on the error tolerance.

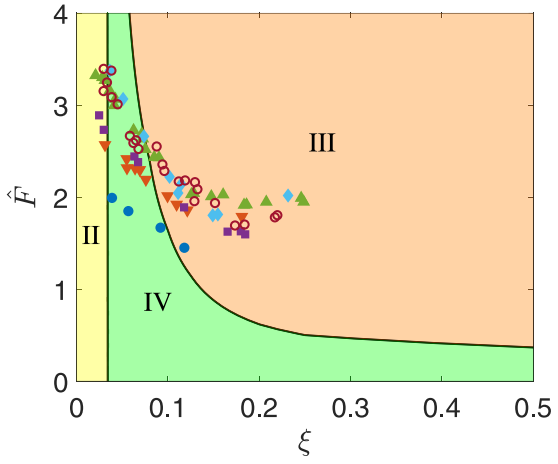

Fig. 8. A model validity map for rubber in the hyperplane $\xi - \hat{F}$. Error tolerances for both $e^{(1)}$ and $e^{(2)}$ are set at 10%. In Region II (yellow), the linear model is acceptable but the incompressible neo-Hookean model is not. In Region III (orange), the incompressible neo-Hookean model is acceptable but the linear model is not. In Region IV (green), both the linear model and the incompressible neo-Hookean model are acceptable. Discrete symbols represent experimental data of critical forces for cavitation in rubber layers from Gent and Lindley (1959). (For interpretation of the references to color in this figure legend, the reader is referred to the web version of this article.)

4. Analysis of PDMS layers

In this section, we construct a model validity map for PDMS layers. We do this by choosing $\nu = 0.49$ for PDMS. In the literature, the value of Poisson's ratio for PDMS ranges from 0.45 to 0.5 (Dogru et al., 2018; Müller et al., 2019). Thus, $\nu = 0.49$ is an acceptable, but certainly not a definitive, choice. But, as far as this paper is concerned, it allows us to compare the cases corresponding to $\nu = 0.49$ versus $\nu = 0.4999$ for rubber. While both can be considered nearly incompressible, the difference between the two cases is significant as far as the ratio κ/μ is concerned, since $\nu = 0.49$ implies

$$\frac{\kappa}{\mu} = 50, \tag{20}$$

which, on the one hand, is significantly larger than one, and, on the other hand, is significantly smaller than that for rubber. Recently, poker-chip specimens with PDMS layers were tested and analyzed by Guo and Ravi-Chandar (2023). Their analysis was based on an incompressible nonlinear model, and the value of κ/μ was not reported.

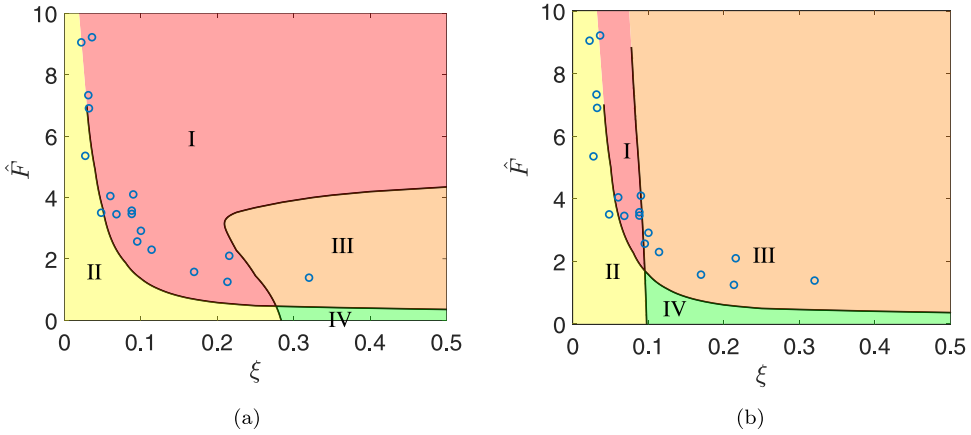

Fig. 9. Model validity maps for PDMS in the hyperplane $\xi - \hat{F}$. (a) $\nu = 0.49$ and (b) $\nu = 0.499$. Error tolerances for both $e^{(1)}$ and $e^{(2)}$ are set at 10%. In Region I (red), neither the linear model nor the incompressible neo-Hookean model is acceptable. In Region II (yellow), the linear model is acceptable but the incompressible neo-Hookean model is not. In Region III (orange), the incompressible neo-Hookean model is acceptable but the linear model is not. In Region IV (green), both the linear model and the incompressible neo-Hookean model are acceptable. The circles represent experimental data of critical forces for onset of cavitation or fracture in PDMS layers from Guo and Ravi-Chandar (2023). (For interpretation of the references to color in this figure legend, the reader is referred to the web version of this article.)

Here we examine the importance of nonlinearity and compressibility in the analysis of PDMS layers by adopting the approach developed in Section 3. Namely, we compute the modeling errors $e^{(1)}$ and $e^{(2)}$ associated with the linear model and the incompressible neo-Hookean model for PDMS, in comparison with the compressible neo-Hookean model. A model validity map for PDMS is shown in Fig. 9(a). It is constructed in the $\xi - \hat{F}$ hyperplane and the error tolerance is set at 10% for both $e^{(1)}$ and $e^{(2)}$. Evidently, the map for PDMS is significantly different from the map for rubber in Fig. 8, constructed using the same error tolerance. In particular, while the contour $e^{(2)} = 0.1$ is nearly vertical for rubber, it is not for PDMS and it is located at much larger ξ values. This difference is due to the much larger compressibility of PDMS in comparison to rubber. Meanwhile, the contours $e^{(1)} = 0.1$ are quite similar for both rubber and PDMS. As a result, the two contours for PDMS intersect at one point on the map, and there are four regions in Fig. 9(a). Notably, while Region I is absent in Fig. 8 for rubber, it dominates Fig. 9(a) for PDMS, where both compressibility and nonlinearity should be considered in the constitutive model.

It may be argued that $\nu = 0.49$ or $\kappa/\mu = 50$ is too small for PDMS. For comparison, we present another model validity map in Fig. 9(b) by using $\nu = 0.499$ or $\kappa/\mu = 500$. As expected, this map differs from both Figs. 8 and 9(a), constructed using the same error tolerance. In particular, the contour $e^{(2)} = 0.1$ is nearly vertical, similar to that in Fig. 8, but it is located at a much larger ξ value (≈ 0.1). Meanwhile, the contours $e^{(1)} = 0.1$ are similar for all three maps. As a result, the two contours intersect at one point on the map, and there are four regions in Fig. 9(b). However, compared to Fig. 9(a), Region I is much smaller. Nevertheless, the effect of compressibility is important for thin layers ($\xi < 0.1$) including Region I and Region II. Therefore, the validity of the approximate models depends sensitively on the value of Poisson's ratio for nearly incompressible materials.

The experimental data from Guo and Ravi-Chandar (2023) are shown as circles on the map (Fig. 9), and each circle represents a critical force associated with the onset of cavitation or fracture in a PDMS layer. Assuming $\nu = 0.49$, the map in Fig. 9(a) shows that the experimental data are mostly located in Region I, where both nonlinearity and compressibility are important. Only for the thickest specimen ($\xi > 0.3$), the incompressible model is acceptable. For the thinnest specimens ($\xi < 0.03$), the linear model is acceptable. Thus, the map in Fig. 9(a) suggests that, as far as poker-chip specimens are concerned, constitutive models for most PDMS layers ($0.03 < \xi < 0.3$) should include both nonlinearity and compressibility. However, if a larger Poisson's ratio is used, the contour $e^{(2)} = 0.1$ shifts left, as shown in Fig. 9(b) for $\nu = 0.499$. Even in this case, a significant portion of the experimental data are located in Region I and Region II, where the effect of compressibility is important.

5. Stress analysis

Since the pioneering works of Gent and Lindley (1957, 1959), poker-chip specimens have been widely used in experimental studies of cavitation and cracking in elastomers (Lindsey, 1967; Iwabe et al., 2000; Fond, 2001; Bayraktar et al., 2008; Kumar et al., 2014; Guo and Ravi-Chandar, 2023). Analysis of such experiments requires reliable constitutive models capable of accurately predicting stresses inside the elastomeric layers. This is essential for identifying critical conditions for the onset of cavitation and crack growth in elastomers.

Since most cavities are typically observed in the center region of the layer, we focus on the normalized mean stress at the center,

$$\hat{\sigma}_m := -\frac{1}{\mu} p(\mathbf{x} = 0)\,, \tag{21}$$

as the quantity of interest. For each material, rubber or PDMS, $\hat{\sigma}_m$ is a function of ξ and $\hat{\Delta}$, for which the modeling errors $e^{(1)}$ and $e^{(2)}$ can be defined in the same way as in Eqs. (18) and (19). Accordingly, we can construct a model validity map in the $\xi - \hat{\Delta}$ hyperplane, and then transform into a map in the $\xi - \hat{\sigma}_m$ hyperplane.

For rubber layers, we present two maps shown in Fig. 10. These maps are constructed using the error tolerances of 1% (Fig. 10(a)) and 10% (Fig. 10(b)) with respect to $\hat{\sigma}_m$. The map in Fig. 10(a) is similar to the one in Fig. 7(b). That is, both maps have four regions and they are similarly shaped. The key difference between these two maps is that the experimental data in Fig. 7(b) are obtained directly from measurements of critical forces, whereas the data in Fig. 10(a) are obtained by converting the critical forces into $\hat{\sigma}_m$ using the compressible neo-Hookean model. As a result of this conversion, for each data, the normalized mean stress at center $\hat{\sigma}_m$ is higher than the normalized axial force $\hat{F}$. On both maps (Figs. 10(a) and 7(b)), almost all data are located in Regions I and III. Therefore, according to these maps, nonlinearity is essential for all the data, whereas compressibility is required for thin layers with $\xi < 0.1$. The map shown in Fig. 10(b) with 10% error tolerance implies a different logic, where Region I is absent, similar to the map in Fig. 8. For very thin layers (in Region II), compressibility is important but nonlinearity is not. For moderately thick layers (in Region III), nonlinearity is important but compressibility is not. And, for intermediate layers (in Region IV), one can use either the linear or incompressible neo-Hookean model.

For PDMS layers, we present one map constructed using $\nu = 0.49$ and the error tolerance of 10% with respect to $\hat{\sigma}_m$ (Fig. 11a). As in the map shown in Fig. 9(a), the experimental data for critical forces are taken from Guo and Ravi-Chandar (2023), and then the corresponding

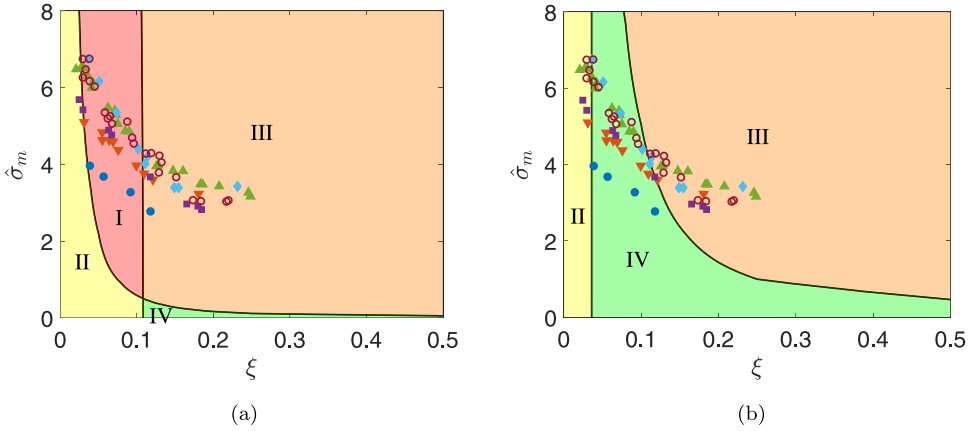

Fig. 10. Model validity maps for rubber in the $\xi - \hat{\sigma}_m$ hyperplane. Error tolerances for $e^{(1)}$ and $e^{(2)}$ are set at (a) 1%, and (b) 10%. In Region I (red), neither the linear nor the incompressible neo-Hookean model are acceptable. In Region II (yellow), the linear model is acceptable but the incompressible neo-Hookean model is not. In Region III (orange), the incompressible neo-Hookean model is acceptable but the linear model is not. In Region IV (green), both the linear model and the incompressible neo-Hookean model are acceptable. Discrete symbols correspond to experimental data of critical forces for onset of cavitation in rubber layers from Gent and Lindley (1959). (For interpretation of the references to color in this figure legend, the reader is referred to the web version of this article.)

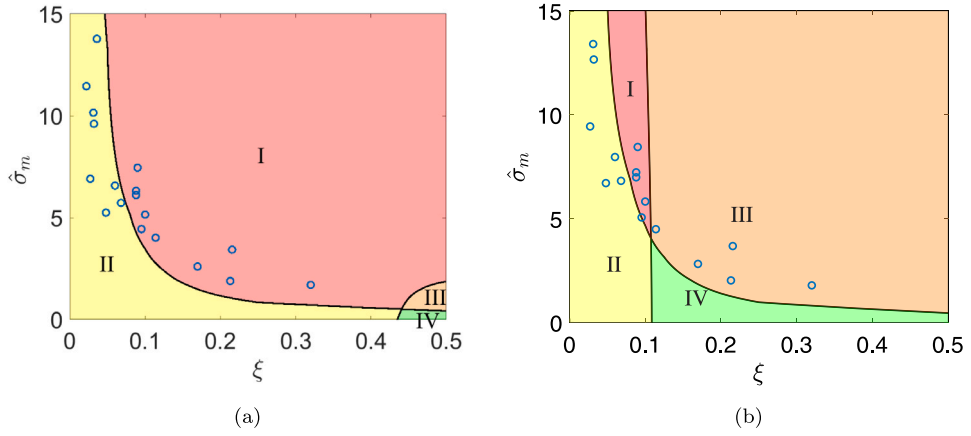

Fig. 11. Model validity maps for PDMS in the $\xi - \hat{\sigma}_m$ hyperplane. (a) $\nu = 0.49$ and (b) $\nu = 0.499$. Error tolerances for both $e^{(1)}$ and $e^{(2)}$ are set at 10%. In Region I (red), neither the linear nor the incompressible neo-Hookean model are acceptable. In Region II (yellow), the linear model is acceptable but the incompressible neo-Hookean model is not. In Region III (orange), the incompressible neo-Hookean model is acceptable but the linear model is not. In Region IV (green), both the linear model and the incompressible neo-Hookean model are acceptable. Discrete symbols correspond to experimental data of critical forces for onset of cavitation or fracture from Guo and Ravi-Chandar (2023). (For interpretation of the references to color in this figure legend, the reader is referred to the web version of this article.)

$\hat{\sigma}_m$ are computed using the compressible neo-Hookean model. According to the map in Fig. 11(a), compressibility is important for analysis of all the data in Guo and Ravi-Chandar (2023). Further, nonlinearity is important for the cases of moderately thick layers ($\xi > 0.1$ roughly) but not for thinner layers. We note that the map in Fig. 11(a) appears quite different from the map in Fig. 9(a), primarily because the contour $e^{(2)} = 0.1$ with respect to $\hat{\sigma}_m$ differs substantially from that with respect to $\hat{F}$ for PDMS. The difference suggests that considering compressibility is more important for the analysis of local stresses than for the overall force–displacement responses of PDMS layers. Again, for comparison, we present another map constructed using $\nu = 0.499$ and the same error tolerance in Fig. 11(b). Similar to Fig. 9(b), a significant portion of the experimental data for PDMS are located in Region I and Region II, where the effect of compressibility is important.

Now we deviate from the mainstream approach of the paper, and focus on predictions based on the compressible neo-Hookean model only. In particular, we are interested in the relationship between $\hat{\sigma}_m$ and $\hat{F}$, which allows one to determine $\hat{\sigma}_m$ in terms of experimentally accessible $\hat{F}$. This relationship is commonly described using the stress concentration factor, namely

$$\text{SCF} := \frac{\hat{\sigma}_m}{\hat{F}}. \tag{22}$$

In general, the SCF depends on ξ, $\hat{F}$, and κ/μ. For a particular material, the SCF is a function of ξ and $\hat{F}$.

Contours of the SCF for rubber ($\nu = 0.4999$) and PDMS ($\nu = 0.49$) are shown in Fig. 12, along with the corresponding experimental data for the critical forces. These contour plots use the $\log \xi - \hat{F}$ rather than $\xi - \hat{F}$ hyperplane, as the logarithmic scale provides a better resolution of the contours, especially for thin layers ($\xi < 0.1$). For rubber (Fig. 12a), the contour lines are nearly vertical for very thin layers ($\xi < 0.02$), as expected from a linear model. For moderately thick rubber layers ($\xi > 0.1$), the SCF increases with $\hat{F}$. For $0.02 < \xi < 0.1$, the SCF varies slightly with $\hat{F}$ and is largely confined in the range $1.9 < \text{SCF} < 2.1$. It is well known that the linear elastic model predicts SCF = 2 for incompressible thin layers ($\xi \ll 1$) but SCF = 1 for compressible thin layers (Lindsey et al., 1963; Lindley, 1979; Qiao and Lu, 2015; Movchan et al., 2021, 2023). For rubber (Fig. 12(a)), except for thicker layers, most of the experimental data are confined to the region $1.9 < \text{SCF} < 2.1$, and thus can be treated approximately as incompressible, linear elastic thin layers. This is consistent with the map in Fig. 10(b), which suggests that the linear model is acceptable for thin layers ($\xi < 0.1$), and compressibility is important only for very thin layers. For thicker layers, nonlinearity is important, and the SCF is lower. As ξ increases further, the linear model predicts that the SCF decreases at small $\hat{F}$

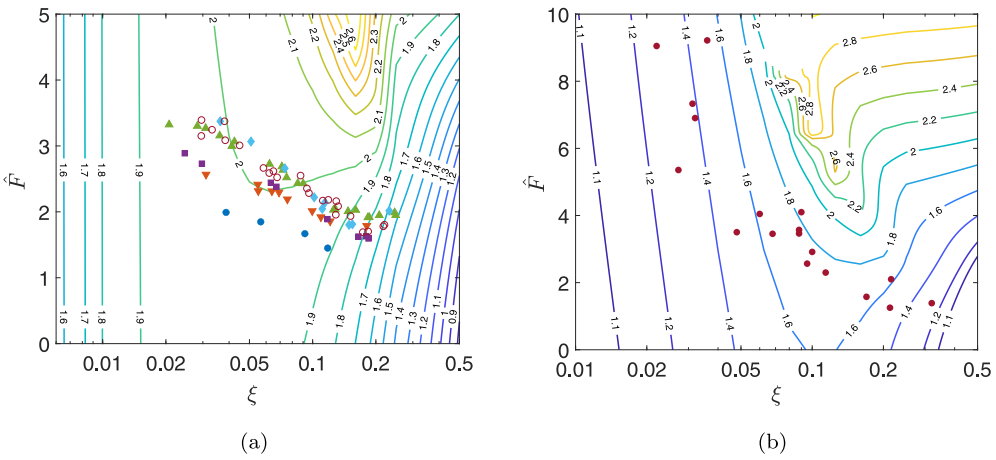

Fig. 12. Contour plots of the stress concentration factor in the $\log\xi - \hat{F}$ hyperplane, for (a) rubber with the experimental data from Gent and Lindley (1959), and (b) PDMS with the experimental data from Guo and Ravi-Chandar (2023).

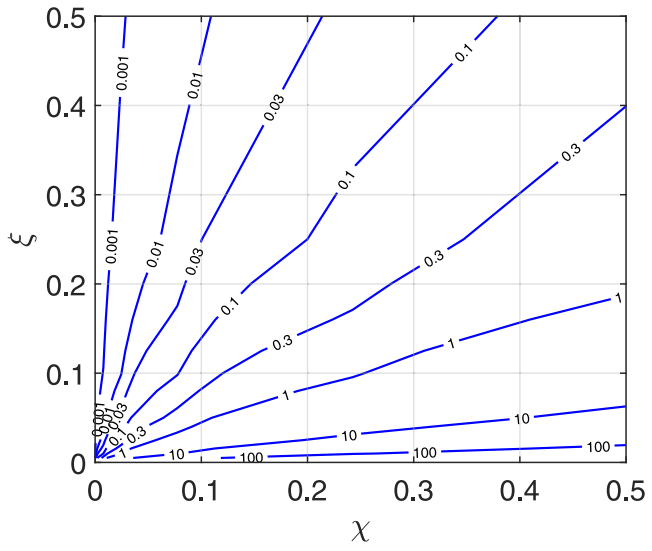

Fig. 13. Contour plot for the modeling error $e^{(2)}$ in the $\chi - \xi$ hyperplane, based on comparing the linear (compressible) model to the linear incompressible one.

and approaches $1/3$ in the limit $\xi \to \infty$, corresponding to the case of uniaxial tension. As $\hat{F}$ increases, the SCF increases for the thicker layers ($\xi > 0.1$) and exceeds 2 when $\hat{F}$ is large. As the thicker layers undergo large deformations, the reduction of the cross-sectional area at the center leads to the increase of the true stress σ_{zz} and correspondingly the SCF.

For PDMS (Fig. 12b), assuming $\nu = 0.49$, the SCF depends on $\hat{F}$ for all layer thinness considered ($0.01 < \xi < 0.5$). At small $\hat{F}$, the SCF is close to 1 for very thin layers ($\xi < 0.01$), as predicted by the linear model in the limit of compressible thin layers. As ξ increases, the SCF first increases and then decreases, with a peak value of around 1.6, much lower than that for rubber. As $\hat{F}$ increases, the SCF increases. The experimental data for the critical forces are scattered in the region $1.2 <$ SCF < 1.9, so that it is neither as compact as the data for rubber layers in Fig. 12(a) nor can be estimated by SCF ≈ 2 as for incompressible, linear elastic thin layers. Thus, in contrast to the rubber layers, the SCF of the PDMS layers is significantly affected by compressibility.

6. The competition parameter

Currently, the majority of widely-used constitutive models for elastomers include nonlinearity but not compressibility. The importance of compressibility, especially for confined PDMS layers, is established in the previous sections, but it is done by fixing the ratio κ/μ. In this section, we examine the role of compressibility by adopting the parameter

$$\chi = \sqrt{\frac{9\mu}{4\kappa + 3\mu}}\,. \tag{23}$$

This parameter was introduced in Lindsey et al. (1963), as it arises naturally from the governing equations of linear elasticity applied to analysis of thin constrained layers. Further, it appeared in many other papers concerned with linear elastic analysis of thin layers (Chalhoub and Kelly, 1990; Tsai and Lee, 1998; Lin et al., 2000; Schapery, 2018a,b; Movchan et al., 2021). It is clear that $\chi = 0$ for incompressible materials; for rubber $\chi = 0.0245$, and for PDMS $\chi = 0.243$ (assuming $\nu = 0.49$).

Movchan et al. (2021) exploited χ for confined thin layers by introducing the parameter

$$\zeta := \frac{\xi}{\chi}\,. \tag{24}$$

We refer to ζ as the competition parameter because, for nearly incompressible (or slightly compressible) materials, it is the ratio of two small parameters, the layer thinness (ξ) and the material compressibility (χ). The competition parameter allows one to identify linear elastic thin layers for which considering compressibility is important, and this identification is not dictated by χ alone, but rather by the competition between the geometric confinement parameter ξ and the material compressibility parameter χ.

According to Movchan et al. (2021), considering compressibility is important for thin layers characterized by $\zeta \ll 1$, but not for thin layers characterized by $\zeta \gg 1$. For example, for rubber ($\chi = 0.0245$), a layer characterized by $\xi = 0.0025$ results in $\zeta \approx 0.1$, and therefore, for such a thin layer, considering compressibility is important. In contrast, for a rubber layer with $\xi = 0.1$, $\zeta \approx 4$, and therefore for such a layer, considering compressibility is not that important. For PDMS ($\chi = 0.243$), however, $\xi = 0.1$ implies $\zeta \approx 0.4$, and therefore for such a PDMS layer, considering compressibility is important.

Let us examine the usefulness of ζ for moderately thick linear elastic layers. To this end, we compute the modeling error $e^{(2)}$ by comparing predictions of the linear incompressible versus linear compressible models. A contour plot for $e^{(2)}$ in the $\chi - \xi$ hyperplane is shown in Fig. 13. In this plot, each contour is close to a ray emanating from the origin. This is consistent with the notion that each contour is associated with a particular value of ζ, and the entire plot can be accurately approximated by $e^{(2)}$ as a function of ζ. Further, numerical values in Fig. 13 support the notion that neglecting compressibility results in

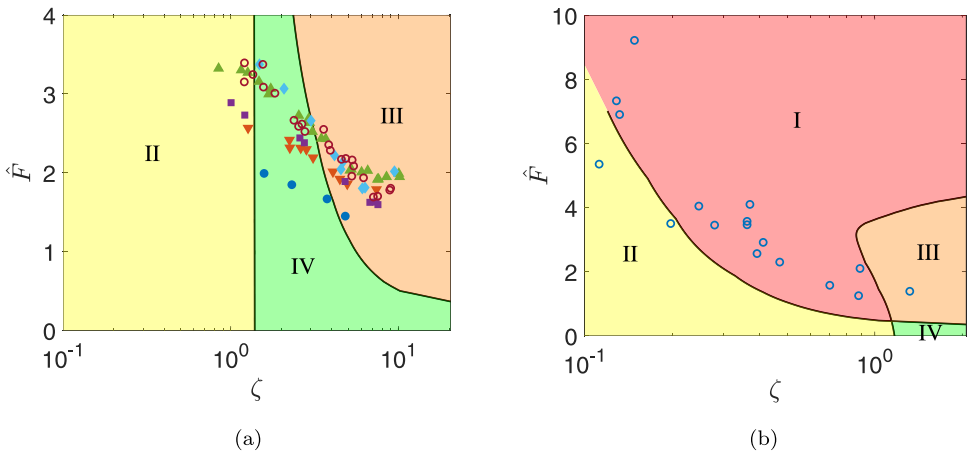

Fig. 14. Model validity maps in the $\log\zeta - \hat{F}$ hyperplane, for (a) rubber ($\nu = 0.4999$) and (b) PDMS layers ($\nu = 0.49$). Error tolerances for both $e^{(1)}$ and $e^{(2)}$ are set at 10%. Discrete symbols are experimental data from Gent and Lindley (1959) for rubber layers, and from Guo and Ravi-Chandar (2023) for PDMS layers.

large errors for layers characterized by small ζ. For example, $\zeta \approx 0.4$ results in $e^{(2)} = 1$. In contrast, $\zeta \approx 5$ results in $e^{(2)} \approx 0.01$.

At this point, let us remove the restriction of linearity and examine the usefulness of ζ in general. We do this by re-scaling the contour plots in Figs. 8 and 9(a) using the $\log\zeta - \hat{F}$ rather than $\xi - \hat{F}$ hyperplane (Fig. 14). The contour plot for rubber (Fig. 14a) shows that the experimental data from Gent and Lindley (1959) correspond to $0.9 < \zeta < 10$. For the error tolerance $e^{(2)} = 0.1$, compressibility is important for $\zeta < 1.5$, but not important for $\zeta > 1.5$. Accordingly, for the experimental data in Fig. 14(a), compressibility is not important except for a few thinnest layers. For PDMS layers, assuming $\nu = 0.49$, the contour plot in Fig. 14(b) shows that the experimental data from Guo and Ravi-Chandar (2023) correspond to $0.1 < \zeta < 2$. For the error tolerance $e^{(2)} = 0.1$, compressibility is important for $\zeta < 1.5$, but not important for $\zeta > 1.5$ at small $\hat{F}$. The importance of compressibility increases with $\hat{F}$ for thicker PDMS layers ($\zeta > 1.5$). Thus, for all the experimental data in Fig. 14(b), ζ is relatively small, so that it is prudent to analyze the data by considering compressibility. The lone data point lying in Region III should not distract from considering compressibility, as the boundary between Regions I and III may shift to the right if the error tolerance is reduced, and the data point may end up in Region I.

7. Summary

In this paper, we analyzed stretching of thin elastomeric layers sandwiched between rigid plates. The purpose of our analysis was to determine conditions under which nonlinearity and compressibility should be considered in the constitutive models. Toward this objective, we evaluated the force–displacement response and the mean stress at the layer center using three constitutive models, one of which was regarded as exact (compressible neo-Hookean), and the other two as approximate. The first approximate model was linear, and the deviation of its prediction from that of the compressible neo-Hookean model was adopted for measuring the importance of nonlinearity. The second approximate model was incompressible neo-Hookean, and the deviation of its prediction from that of the compressible neo-Hookean model was adopted for measuring the importance of compressibility. These models were applied to rubber and PDMS layers, and the results were compared with the experimental data for rubber (Gent and Lindley, 1959) and PDMS (Guo and Ravi-Chandar, 2023). It was concluded that, in general, considering nonlinearity is more important for thicker layers, and considering compressibility is more important for thinner layers. Specifically, considering compressibility is important for analyzing the data for thin rubber layers and nearly all PDMS layers considered. This contradicts the common practice of modeling both materials as incompressible.

The importance of considering nonlinearity in constitutive models for elastomers has been firmly established in the literature. In contrast, compressibility is often neglected, and our analysis challenges the validity of this assumption, at least for such confined layers as in poker-chip specimens. In this regard, we evaluated the usefulness of the parameter ζ (Movchan et al., 2021), which describes the competition between the layer thinness ξ and the material compressibility χ. Results of our analysis are summarized as follows:

- For $\zeta \ll 1$, considering compressibility is very important.
- For $\zeta \gg 1$, considering compressibility is not important.
- For a large fraction of experimental data for rubber (Gent and Lindley, 1959) and PDMS (Guo and Ravi-Chandar, 2023), $\zeta = \mathcal{O}(1)$, and therefore it is prudent to analyze the data by considering compressibility. A notable exception here is for the case of a moderately thick rubber layer.

Let us conclude by emphasizing that, in this work, we do not advocate for the compressible neo-Hookean model per se. To the contrary, we hope that, in the future, the approach presented here will be applied to more accurate models for specific materials. To this end, let us mention that we applied our approach to rubber layers using the Mooney–Rivlin model, and obtained results that were practically indistinguishable from those obtained with the neo-Hookean model.

CRediT authorship contribution statement

Sida Hao: Writing – original draft, Visualization, Validation, Methodology, Investigation, Data curation. **Rui Huang:** Writing – review & editing, Visualization, Validation, Supervision, Methodology, Investigation, Conceptualization. **Gregory J. Rodin:** Writing – review & editing, Visualization, Validation, Methodology, Investigation, Conceptualization.

Declaration of competing interest

The authors declare that they have no known competing financial interests or personal relationships that could have appeared to influence the work reported in this paper.

Data availability

Data will be made available on request.

Acknowledgments

The authors acknowledge Prof. K. Ravi-Chandar and Jinlong Guo of the University of Texas at Austin for helpful discussions and the experimental data provided for PDMS layers. S.H. and R.H. gratefully acknowledge financial support by the Portuguese Foundation for Science and Technology – FCT under the UT Austin Portugal program through the project Soft4Sense. G.J.R. acknowledges the support by the project MCTool[21] (6305-1452/1490) co-financed by the European Regional Development Fund through the Operational Program for Competitiveness and Internationalization COMPETE 2020, the North Portugal Regional Operational Program NORTE 2020, and by the Portuguese Foundation for Science and Technology FCT under the UT Austin Portugal Program.

References

Anand, L., Govindjee, S., 2020. Continuum Mechanics of Solids. Oxford University Press.
Anderson, M.L., Mott, P.H., Roland, C.M., 2004. The compression of bonded rubber disks. Rubber Chem. Technol. 77 (2), 293–302.
Auslender, F., Trifa, M., Sidoroff, F., 1999. Material compressibility effects for the squeeze of very thin films. Eur. J. Mech./A Solids 18 (3), 499–515.
Basar, Y., Weichert, D., 2000. Nonlinear Continuum Mechanics of Solids: Fundamental Mathematical and Physical Concepts. Springer Science & Business Media, pp. 160–162.
Bayraktar, E., Bessri, K., Bathias, C., 2008. Deformation behaviour of elastomeric matrix composites under static loading conditions. Eng. Fract. Mech. 75 (9), 2695–2706.
Benvidi, F.H., Bacca, M., 2021. Theoretical limits in detachment strength for axisymmetric bi-material adhesives. J. Appl. Mech. 88 (12), 121007.
Chalhoub, M.S., Kelly, J.M., 1990. Effect of bulk compressibility on the stiffness of cylindrical base isolation bearings. Int. J. Solids Struct. 26 (7), 743–760.
Dogru, S., Aksoy, B., Bayraktar, H., Alaca, B.E., 2018. Poisson's ratio of PDMS thin films. Polym. Test. 69, 375–384.
Fischer, S.C., Arzt, E., Hensel, R., 2017. Composite pillars with a tunable interface for adhesion to rough substrates. ACS Appl. Mater. Interfaces 9 (1), 1036–1044.
Fond, C., 2001. Cavitation criterion for rubber materials: A review of void-growth models. J. Polym. Sci. B 39, 2081–2096.
Gent, A.N., 1990. Cavitation in rubber: a cautionary tale. Rubber Chem. Technol. 63 (3), 49–53.
Gent, A.N., 1994. Compression of rubber blocks. Rubber Chem. Technol. 67 (3), 549–558.
Gent, A.N., Lindley, P.B., 1957. Internal flaws in bonded cylinders of soft vulcanized rubber subjected to tensile loads. Nature 180, 912–913.
Gent, A.N., Lindley, P.B., 1959. Internal rupture of bonded rubber cylinders in tension. Proc. R. Soc. Lond. Ser. A 249 (1257), 195–205.
Guo, J., Ravi-Chandar, K., 2023. On crack nucleation and propagation in elastomers: I. In situ optical and X-ray experimental observations. Int. J. Fract. 243, 1–29.
Hao, S., Suo, Z., Huang, R., 2023. Why does an elastomer layer confined between two rigid blocks grow numerous cavities? J. Mech. Phys. Solids 173, 105223.
Hensel, R., McMeeking, R.M., Kossa, A., 2019. Adhesion of a rigid punch to a confined elastic layer revisited. J. Adhes. 95 (1), 44–63.
Iwabe, N., Takayama, M., Kani, N., Wada, A., 2000. Experimental study on the effect of tension for rubber bearings. In: 12th World Conference on Earthquake Engineering. Auckland, New Zealand, p. 1290.
Kelly, J.M., Konstantinidis, D., 2011. Mechanics of Rubber Bearings for Seismic and Vibration Isolation. John Wiley & Sons.
Klingbeil, W.W., Shield, R.T., 1966. Large-deformation analyses of bonded elastic mounts. Z. Angew. Math. Phys. ZAMP 17, 281–305.
Kumar, A., Lopez-Pamies, O., 2021. The poker-chip experiments of Gent and Lindley (1959) explained. J. Mech. Phys. Solids 150, 104359.
Kumar, M., Whittaker, A.S., Constantinou, M.C., 2014. An advanced numerical model of elastomeric seismic isolation bearings. Earthq. Eng. Struct. Dyn. 43 (13), 1955–1974.
Lefèvre, V., Ravi-Chandar, K., Lopez-Pamies, O., 2015. Cavitation in rubber: an elastic instability or a fracture phenomenon? Int. J. Fract. 192, 1–23.
Lin, Y., Hui, C., Conway, H., 2000. A detailed elastic analysis of the flat punch (Tack) test for pressure-sensitive adhesives. J. Polym. Sci. B – Polym. Phys. 38 (21), 2769–2784.
Lindley, P.B., 1979. Compression moduli for blocks of soft elastic material bonded to rigid end plates. J. Strain Anal. Eng. Des. 14 (1), 11–16.
Lindsey, G.H., 1967. Triaxial fracture studies. J. Appl. Phys. 38, 4843–4852.
Lindsey, G.H., Schapery, R.A., Williams, M.L., Zak, A.R., 1963. The Triaxial Tension Failure of Viscoelastic Materials. Technical Report 63–152, Aerospace Research Laboratories.
Minsky, H., Turner, K., 2015. Achieving enhanced and tunable adhesion via composite posts. Appl. Phys. Lett. 106, 201604.
Movchan, A.B., Movchan, N.V., Rodin, G.J., 2023. Asymptotic analysis of thin linear elastic layers constrained by two rigid plates. Int. J. Solids Struct. 285, 112561.
Movchan, A.B., Rebrov, K.R., Rodin, G.J., 2021. Axisymmetric deformation of compressible, nearly incompressible, and incompressible thin layers between two rigid surfaces. Int. J. Solids Struct. 214, 61–73.
Müller, A., Wapler, M.C., Wallrabe, U., 2019. A quick and accurate method to determine the Poisson's ratio and the coefficient of thermal expansion of PDMS. Soft Matter 15 (4), 779–784.
Ogden, R.W., 1997. Non-Linear Elastic Deformations. Dover Publications.
Pence, T.J., Gou, K., 2015. On compressible versions of the incompressible neo-Hookean material. Math. Mech. Solids 20 (2), 157–182.
Qiao, S., Lu, N., 2015. Analytical solutions for bonded elastically compressible layers. Int. J. Solids Struct. 58, 353–365.
Reynolds, O., 1886. On the theory of lubrication and its application to Mr. Beauchamp Tower's Experiments, including an experimental determination of the viscosity of Olive Oil. Philos. Trans. R. Soc. Lond. Ser. A 177 (300–311), 157–234.
Schapery, R.A., 2018a. Elastomeric bearing sizing analysis Part 1: Spherical bearing. Int. J. Solids Struct. 152, 118–139.
Schapery, R.A., 2018b. Elastomeric bearing sizing analysis Part 2: Flat and cylindrical bearings. Int. J. Solids Struct. 152, 140–150.
Stefan, J., 1874. Versuche über die scheinbare adhäsion. Sitzungsberichte Kais. Akad. Wiss. Math.-Naturwissenschaftliche Cl. 69 (2), 713–735.
Stringfellow, R., Abeyaratne, R., 1989. Cavitation in an elastomer: Comparison of theory with experiment. Mater. Sci. Eng. A 112, 127–131.
Tsai, H.-C., Lee, C.-C., 1998. Compressive stiffness of elastic layers bonded between rigid plates. Int. J. Solids Struct. 35 (23), 3053–3069.
Warn, G.P., Ryan, K.L., 2012. A review of seismic isolation for buildings: historical development and research needs. Buildings 2 (3), 300–325.
Webber, R.E., Shull, K.R., Roos, A., Creton, C., 2003. Effects of geometric confinement on the adhesive debonding of soft elastic solids. Phys. Rev. E 68 (2), 021805.